International Journal of Recent Technology and Engineering (IJRTE)
ISSN: 2277-3878 (Online), Volume-8 Issue-6, March 2020

Estimation of Geodynamic Properties using Seismic Techniques at a Steel Rolling Factory, Northwestern Gulf of Suez, Egypt

Maher A.Mesbah, Asem Salama, Mohamed A. Albarqawy, Eslam M.Ali

Abstract*: The objective of the current investigations is to estimate the dynamic geotechnical properties necessary for evaluating the conditions of the subsurface in order to make better decisions for economic and safe designs of the proposed structures at a Steel Rolling Factory, Ataqa Industrial Area, Northwestern Gulf of Suez, Egypt. To achieve this purpose, four seismic refraction profiles were conducted to measure the velocity of primary seismic waves (P-waves) and four profiles were conducted using Multichannel Analysis of Surface Waves (MASW) technique in the same locations of refraction profiles to measure the velocity of shear waves (S-waves). SeisImager/2D Software Package was used in the analysis of the measured data. Data processing and interpretation reflect that the subsurface section in the study area consists of two layers, the first layer is a thin surface layer ranges in thickness from 1 to 4 meters with P-wave velocity ranges from 924 m/s to 1247 m/s and S-wave velocity ranges from 530 m/s to 745 m/s. The second layer has a P-wave velocity ranges from 1277 m/s to 1573 m/s and the S-wave velocity ranges from 684 m/s to 853 m/s. Geotechnical parameters were calculated for both layers. Since elastic moduli such as Poisson's ratio, shear modulus, Young's modulus, and bulk's modulus were calculated. Competence scales such as material index, stress ratio, concentration index, and density gradient were calculated also. In addition, the ultimate and allowable bearing capacities.

***Keywords*: Seismic refraction; MASW; Geotechnical properties; Elastic moduli**

I. INTRODUCTION

The area under investigation is a steel rolling factory. Which is one of the leading corporations in the steel industry; it has an ambitious plan for a new project at the escarpment of Ataqa Mountain in Ataqa Industrial Area, Suez "Fig. 1". Different constructions are proposed such as control buildings, transformers, and gas-insulated substation buildings. This study aims to evaluate the subsurface geotechnical conditions at the site and develops the essential criteria and parameters required for the design and construction of the foundations of the proposed constructions. In large engineering projects such as high rising buildings, factories, dams, highways, and bridges, the greatest risk comes from the uncertainties related to subsurface conditions [1].

Obtaining adequate and accurate information about the subsurface conditions is an essential first task for understanding and evaluating the conditions of the subsurface in order to make better decisions for a more economical and safe design of the proposed structures. Thus, geotechnical investigations or so-called site investigations are carried out [2].

Boreholes, trenches and other invasive methods such as standard penetration test and cone penetration test are conventionally used to investigate the subsurface. Although these geotechnical methods provide accurate data; but sometimes fail to define weak deposits like soft clay.

They are also considered expensive, time-consuming [3], discrete localized and only yield point information which means sampling small volume of the material only. Although their accuracy is lower than that of the geotechnical methods, geophysical techniques are fast, cost-effective, and provide more continuous information on the subsurface[4]. Generally, most geophysical methods are non-destructive techniques.

Seismic refraction is a non-intrusive and non-destructive geophysical method, which provides a faster and more convenient method of subsurface assessment by determining the actual P-wave velocity, elastic and bearing strength of near-surface that is suitable for sustaining engineering structures [5],[6] Also, multichannel analysis of surface waves (MASW) method is considered one of the most common non-invasive and non-destructive methods used for site assessment by measuring the shear wave velocity distribution in the subsurface [7].

In the current study, we applied both seismic refraction and MASW techniques by conducting four seismic profiles at the same locations. After applying the "Time Term Inversion" technique in processing and interpretation using Seisimager software, we managed to measure both P- and S-waves seismic velocity for the near-surface layers. The measured velocities were used to calculate the different geotechnical parameters of the near subsurface at the study area which was found to be suitable for proposed constructions.

Manuscript received on February 10, 2020.
Revised Manuscript received on February 20, 2020.
Manuscript published on March 30, 2020.
* Correspondence Author
Maher A.Mesbah Faculty of Petroleum and Mining Engineering, Suez University, Suez, Egypt.
Asem Salama, National Research Institute of Astronomy and Geophysics (NRIAG), Helwan, Egypt.
Mohamed A. Albarqawy, Faculty of Petroleum and Mining Engineering, Suez University, Suez, Egypt.
Eslam M.Ali *, Faculty of Petroleum and Mining Engineering, Suez University, Suez, Egypt.

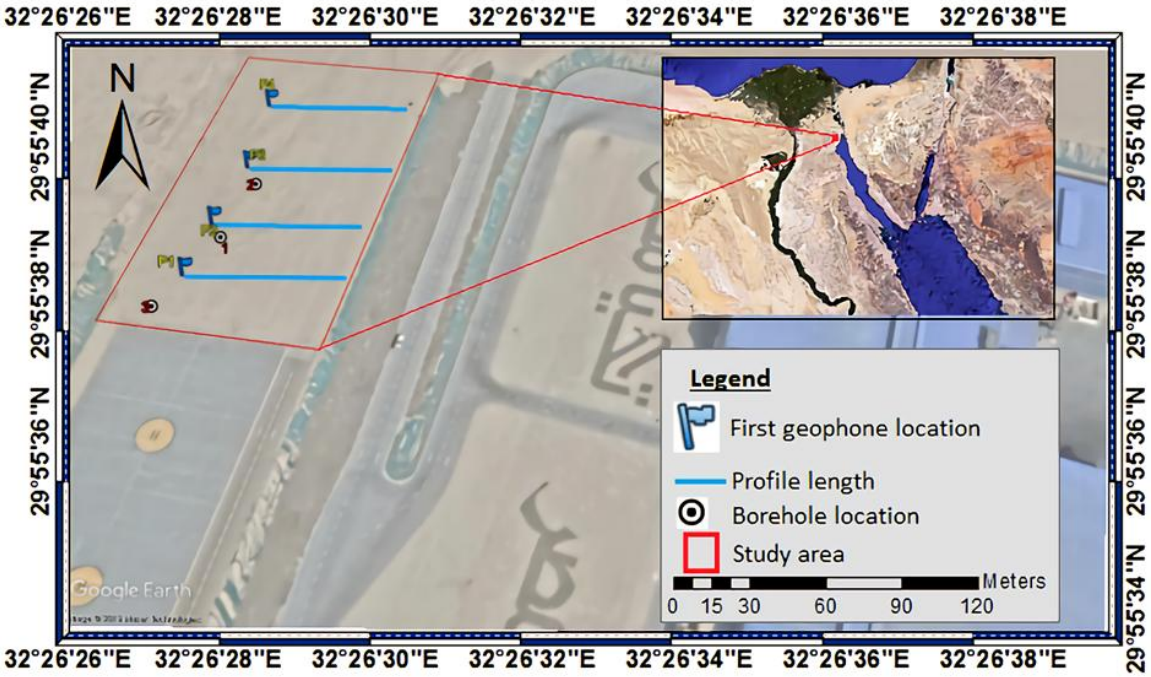

Fig.1. The location of the study area and the distribution of the primary seismic refraction, MASW profiles, and boreholes location.

II. GEOLOGIC SETTING

The surface geology of the Northwestern Gulf of Suez area as shown in "Fig.2" has been described by many authors such as [8][9][10][11][12]. These studies summarized the surface geology of the area as follows: **(i)Eocene rocks** which are divided into the middle and upper Eocene rocks: **(A) the middle Eocene rocks** are covering the northern part of the area and are represented by a succession of limestone in Okheider Mountain. On the other hand, **(B) the upper Eocene rocks** are exposed at the low southern margins of Ataqa Mountain and consist of clay, marl and fossiliferous calcareous sandstone.

(ii)Oligocene rocks exist below the southern margins of Ataqa Mountain and below the eastern margins of Kaheilia and Um Zeita Mountains. These rocks consist of **(iii)Miocene rocks** are divided into middle Miocene rock units and upper Miocene rocks: **(A)the middle Miocene rock units** are of shallow marine origin and are occupying the greatest part cropped out in the area, while **(B) the upper Miocene rocks** consist of white to yellow calcareous sandstone, and extend between Wadi Hagoul and Wadi El Badaa.

(iv)Quaternary deposits are represented by the recent deposits, which covered the coastal plain, wadis, and the low areas below the surrounding mountains until reaching the shoreline. These deposits include alluvium, wadi deposits, and coastal sand and sabkha: **(A)alluvium deposits** consist of big gravel boulders of limestone mixed with sand and gypsum. **(B)Wadi deposits** consist of calcareous boulders covering the surface of the wadis near the mountains of Akheider, El Galala El Bahariya, Ataqa, Kaheilia, and Um Zeita. **(C)Coastal sand and Sabkha** cover parts of the coastal sands are wet by seawater forming salty deposits.

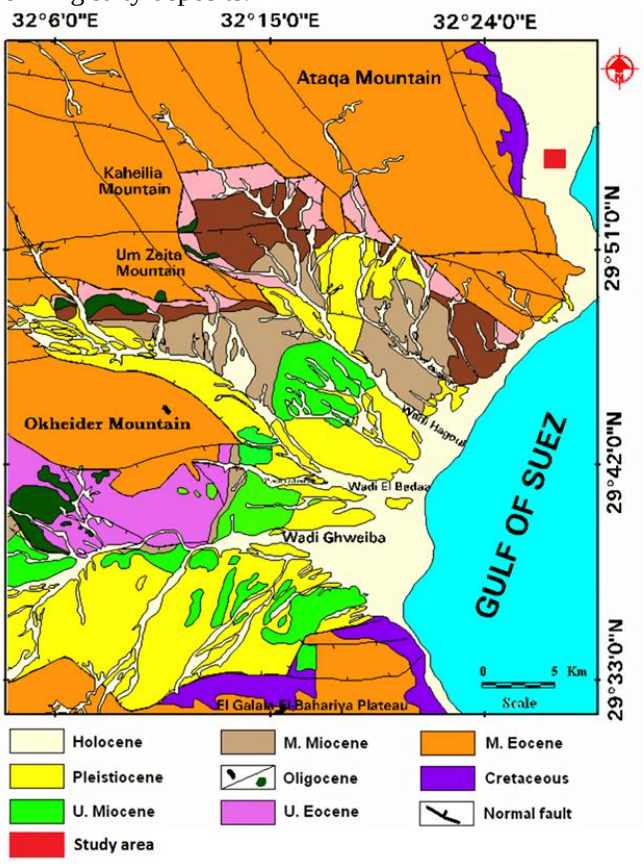

Fig.1. Geological map of Northwestern Gulf of Suez area[8].

III. METHODOLOGY

The study area is located between latitudes 29°55'37.34"N and 29°55'41.46"N, and longitudes 32°26'25.55"E and 32°26'28.53"E with an approximate area of 10,652 m^2 at the escarpment of Ataqa Mountain in the corner zone of the Steel Rolling Factory, Ataqa Industrial Area, Suez as shown in "Fig.1"

A. Seismic refraction method

For the acquisition of shallow seismic refraction data, four profiles were conducted in the "W-E" direction using the 24-channel SmartSeis Exploration Seismograph manufactured by GEOMETRICS Company in order to measure P-wave seismic velocity. The length of each profile was 55 m using 12 vertical geophones of 14 Hz natural frequency with a geophone interval of 5 m. A 15 kg weight hammer and a 30 cm in diameter metallic plate were used as a source to generate the seismic waves. The shot locations for each profile were at an offset five meters from both ends and at the midpoint. Three to five stacks were made per each shot in order to enhance the data quality and increase signal to noise ratio. A sampling rate of 0.250 ms and a recording length of 500 ms were used.

B. Multichannel analysis of surface waves (MASW) method

The acquisition of MASW profiles was accomplished using the 24-channel SmartSeis Exploration Seismograph. A 15 kg weight hammer and a 30 cm in diameter metallic plate were used to generate the seismic waves. Three to five stacks were made per shot. A sampling rate of 0.5ms and a recording length of 1000 ms were adopted. Four 1D profiles were carried out in the same locations of refraction profiles. The length of every profile was 55m using 12 vertical geophones of 4.5 Hz natural frequency with a geophone interval of 5m.

C. Geotechnical investigations

Three boreholes were drilled by [13] to a depth of 15 m from the ground surface at each borehole location. Several soil samples were taken for laboratory tests and analyses such as specific gravity, grain size distribution, and chemical analysis to emphasize the lithologic description of the subsurface. The locations of the drilled boreholes are mentioned in "Fig.1" and the lithologic description is shown in "Fig.3".

IV. DATA PROCESSING

The stage of seismic data processing and interpretation was implemented using SeisImager/2D Software Package (Pickwin version 5.8.0.3 2018, Plotrefa version 3.3.0.0 2018 and waveEq. version 4.6.1.1).

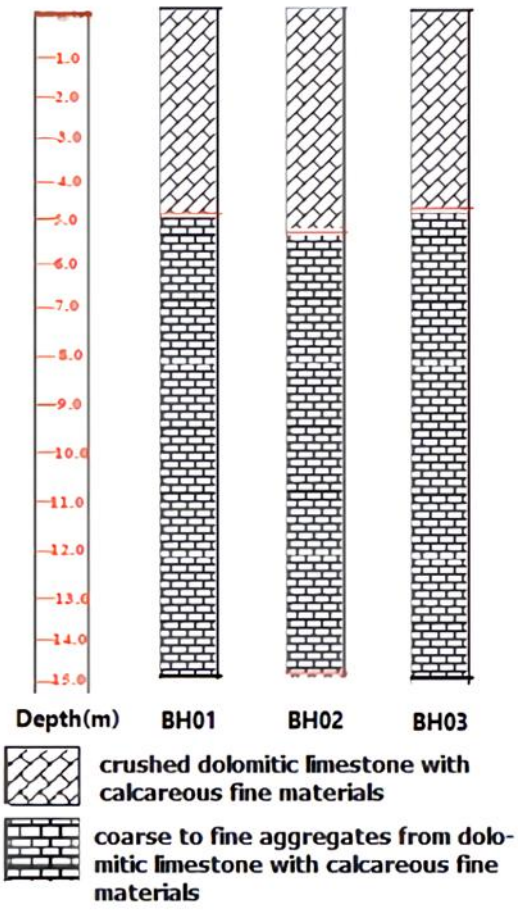

Fig.3. Lithologic description obtained from previously drilled boreholes in the study area.

A. Seismic refraction data

In this study, "Time-term inversion" technique which employs a combination of delay time and linear least squares[14]. This technique is a quick and easy way to estimate the refractor depth by assuming that the subsurface is vertically stratified and does not account for the lateral changes. "Equation (1)" is the general equation used by the "Time-term inversion" technique [15]:

$$t_j = \sum_{k=1}^{n} 2Sjk\ cos(ic)\ Zk + Xj\ S2 \qquad (1).$$

Where, (t) is the total travel time from source to receiver, (n) is the number of receivers, (S) is the "slowness" which equals the inverse of the velocity, (i_c) is the critical angle of refraction, (Z) is the vertical distance to the refractor, and (X) the offset between the source and the receiver.

The first step of seismic refraction data processing is the accurate picking of the first breaks corresponding to the geophones in the profile using the Pickwin module, then the time-distance curve for the profile is generated based on the profile length, geophone spacing, shooting locations, and the first arrival times. The second step is performed by analyzing the generated time-distance curves using the Plotrefa module. The time-distance curves are edited, corrected

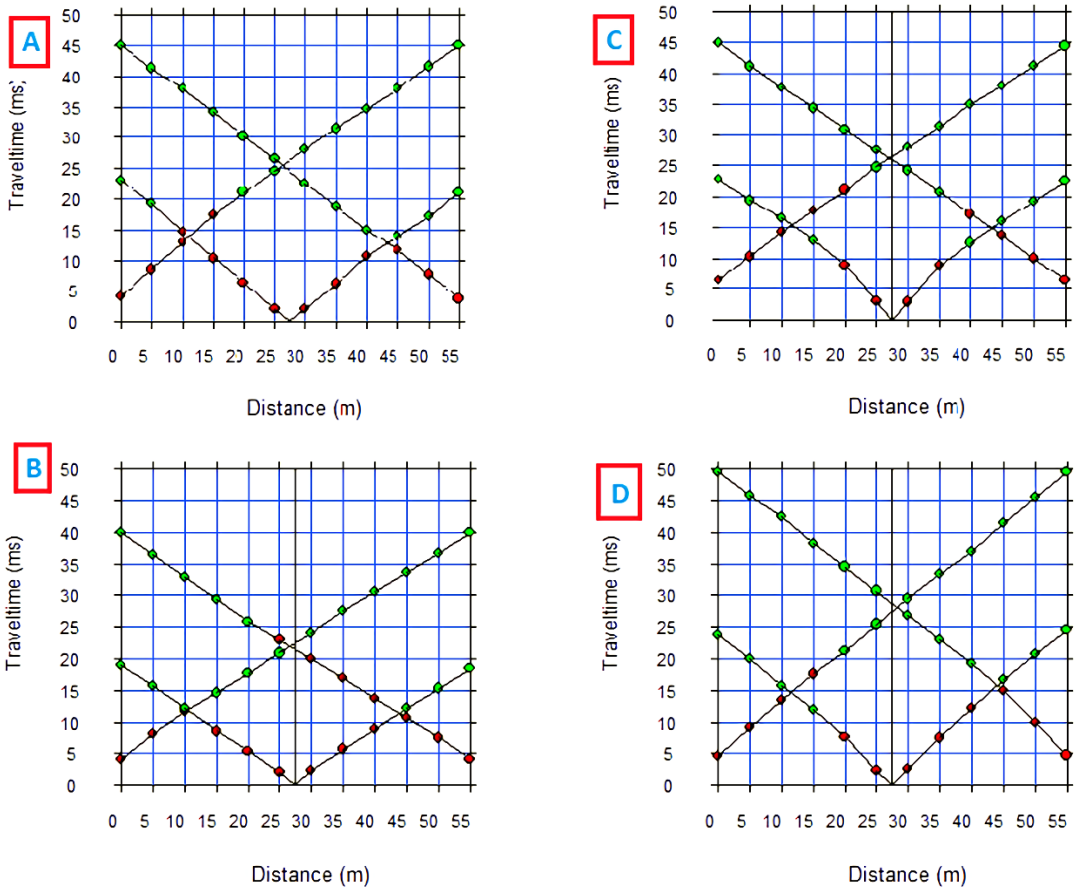

Fig.4. The time-distance curves (A) for profile1, (B) for profile2, (C) for profile3 and (D) for profile4.

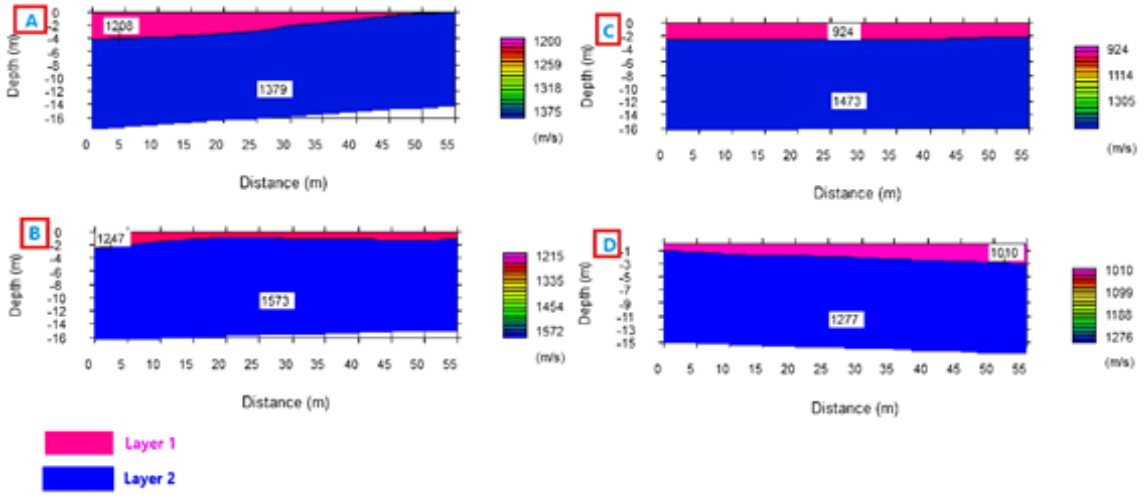

Fig. 5 the 2D velocity-depth models(A) for profile1, (B) for profile2, (C) for profile3 and (D) for profile4.

and checked for estimating the P-wave velocity. The final step is creating the final velocity-depth model for the corresponding time-distance curve using one of the inversion techniques provided by the Plotrefa module. The root mean square error (RMSE) of our final velocity-depth profiles is less than (0.5%) indicating a very good fit between the observed and calculated travel- times. The time-distance curves are shown in (Fig.4) and the corresponding 2D velocity-depth models are shown in "Fig.5"

B. Multichannel analysis of surface waves (MASW) method.

The processing of MASW data is based on the concept of the dispersion of seismic waves. In general, seismic velocity increases with depth, the shorter wavelengths propagate slower than the longer wavelengths, so the frequency content of the wave disperses with the transit time so, the dispersion curve is a relationship between the phase velocities of seismic waves with the corresponding frequencies. During data processing, the MASW approach does not aim to identify the individual dispersion curves but attempts to construct an overall image space where trends can be identified[16], [17].

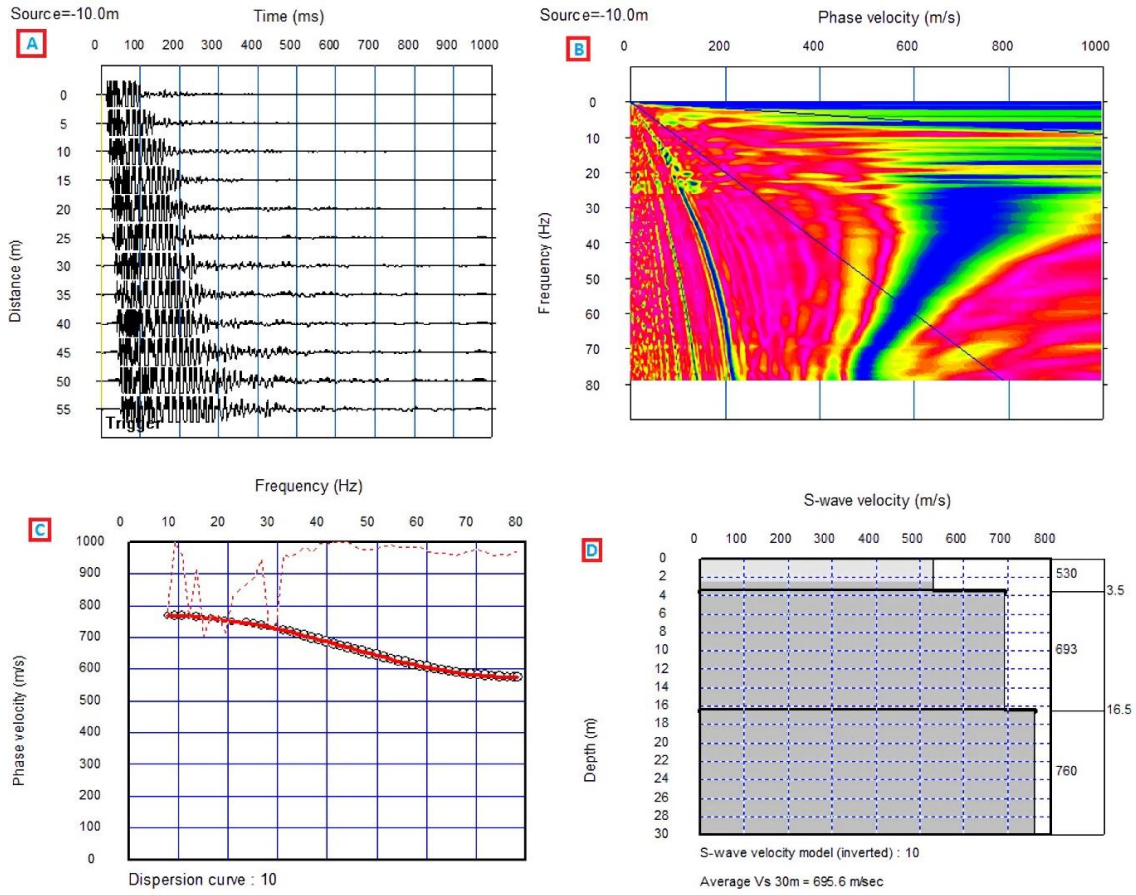

Fig.2 The procedure of MASW data processing using SeisImager software, a) detection of surface waves, b) image of dispersion curve, c) inversion of dispersion curve, d) 1D shear wave velocity profile.

In this study, the MASW raw data were analyzed and processed by using SeisImager/SW modules. The first step is to display and visualize the waveform record using the Pickwin module as shown in "Fig.6a". The second step is to develop the dispersion curve which is considered one of the most critical steps for generating an accurate shear-wave velocity profile. This step starts by selecting the frequency domain which in this study ranges from 5 to 80Hz. Considering the offset-time (x-t) domain is represented by u(x,t) of a shot gather, the Fourier transformation applied to the time axis of u(x,t) to obtain distance-frequency domain U(x,ω) is[18]:

$$U(x,\omega) = \int u(x,t)\, e^{t\omega t}\, dt. \qquad (2).$$

In U(x,ω), each frequency component is separated from other frequencies and the information of the arrival time is preserved in the phase spectrum. Then, the phase velocity-frequency F(c,ω) plot is displayed as shown in "Fig.6b" by applying the following integral transformation to U(x,w) which is called phase shift stack[18], [19]:

$$F(c,\omega) = \int U(x,\omega) e^{i\omega x/c} dx. \qquad (3).$$

The third step comes when the WaveEq module starts and the dispersion curve is displayed as shown in "Fig.6c". The dispersion curve is edited as needed to eliminate noisy picks on the low and high-frequency ends of the curve. The final step is to set up the initial model of shear wave velocity with depth and set the suitable number of iterations for the data inversion to converge on the best fit of the initial model with the observed data and the final1D S-wave velocity profile is displayed as shown in "Fig.6d" The root mean square errors (RMSE) of our final velocity-depth profiles are less than (5%).

V. RESULTS

Results of processing primary seismic refraction and MASW data show that the final velocity-depth models in most of the profiles in the study area represent two layers "Fig.5". The first layer is a thin surface layer ranges in thickness from 1 to 4 meters with P-wave seismic velocity ranges from 924 m/s to 1247 m/s and S-wave velocity ranges from 530 m/s to 745 m/s. This layer is corresponding to the surface deposits composed of offwhite to grey layer from crushed dolomitic limestone with calcareous fine materials. The second layer has a P-wave seismic velocity ranges from 1277 m/s to 1573 m/s and S-wave velocity ranges from 684 m/s to 853 m/s. This layer is corresponding to the deposits composed of offwhite to brown layer from coarse to fine aggregates of dolomitic limestone with fine calcareous sediments.

The final depth-velocity models are represented in two forms: (1) Vertical depth-velocity models, which display vertical distributions of each detected layer "Fig.5a-d". and (2) Velocity contour maps, which show the lateral distribution over the study area. Velocity contour maps for both p- wave and S-wave are generated for the first and the second layer

"Figs.7&8".

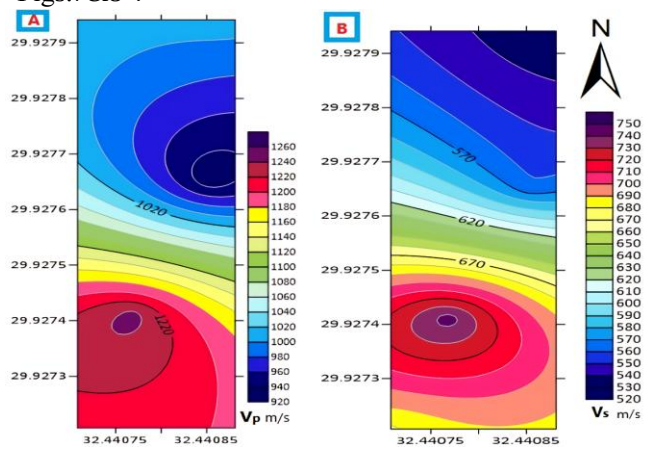

Fig. 7 (A): Contour map illustrates the compressional (P) wave velocity of the first layer. (B): Contour map illustrates the shear (S) wave velocity of the first layer.

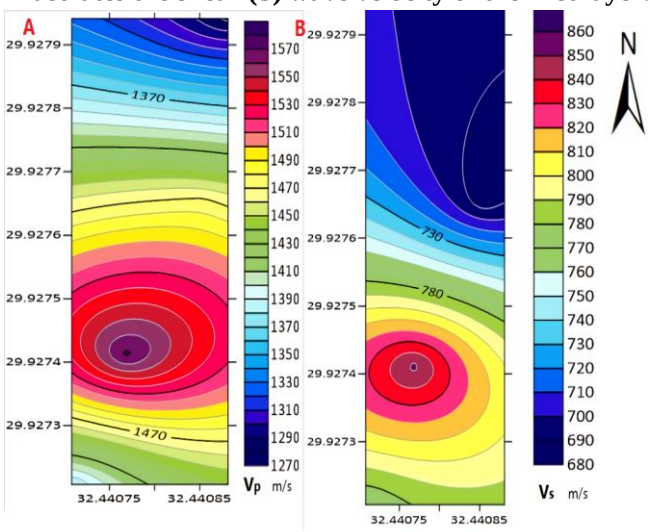

Fig. 8 (A): Contour map illustrates the compressional (P) wave velocity of the second layer. (B): Contour map illustrates the shear (S) wave velocity of the second layer.

VI. GEOTECHNICAL CHARACTERISTICS

To compute the various engineering parameters, the P-wave velocity, and S-wave velocity values are measured from the acquired seismic refraction and MASW profiles respectively then the elastic moduli such as Poisson's ratio, bulk's modulus, shear modulus, and Young's modulus of subsurface materials are calculated from the measured P-wave velocity, and S-wave velocity. Competence scales such as material index, concentration index and stress ratio, and density gradient and ultimate and allowable bearing capacities are then calculated. The integration of these parameters is used to assess the suitability of a site for construction activities.

A. Bulk density

We first calculate the density of soil using the following empirical equation given by [20] and defines the relationship between the increase in P-wave velocity and the bulk density.

$$\rho = a * V_P^{0.25} \qquad (4).$$

where: ρ is the density in g/cm3, VP is the P-wave velocity in m/s and (a) is a constant equals 0.31. According to this formula, the bulk density values- for the first layer in the area under investigation- range from 1.71 gm/cm^3 to 1.84 gm/cm^3 "Fig.9a". and for the second layer the bulk density range from 1.85 gm/cm^3 to 1.9 gm/cm^3 "Fig.9b".

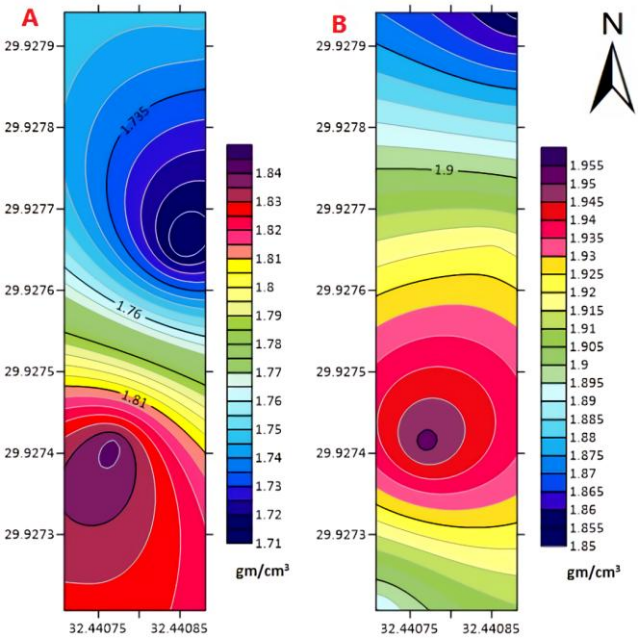

Fig. 9 (A): Contour map illustrates the bulk density of the first layer. (B): Contour map illustrates the bulk density of the second layer.

B. Elastic moduli

Elastic moduli for the subsurface are considered very important parameters to evaluate any site for different construction purposes.

- **Poisson's ratio (σ).**

Poisson's ratio (σ) is defined as the ratio of lateral strain to longitudinal strain where high competent rocks possess lower Poisson's ratio and vice versa. We calculated Poisson's ratio (σ) using the following equation given by [20],[21]:

$$\sigma = \frac{(Vp/Vs)^2 - 2}{2(Vp/Vs)^2 - 2} \qquad (5).$$

Where Vp and V_S are the compressional and shear wave velocities in m/s respectively. [22] summarised the soil properties for construction purposes into four main categories "Table.1" depending on its Poisson's ratio and the material index. In this study, the Poisson's ratio (σ) of the first layer "Fig.10a" has values ranging from 0.206 to 0.310 while, in the second layer Poisson's ratio (σ) "Fig.11a" ranges from 0.274 to 0.363 which, reflects fairly to moderately competent rock.

- **Shear modulus (μ).**

[23] estimated the shear modulus (μ) in terms of shear wave velocity (V_S), density (ρ) as follows:

$$\mu = \rho * V_S^2 \qquad (6).$$

Where (ρ) is the layer density in gm/cm^3, (Vs) is the shear wave velocity in m/sec and (μ) is the Shear modulus in Pascal. In the present study, the shear modulus (μ) exhibits values from 0.49 GPa to 1.02 GPa in the first layer "Fig.10b" while in the second layer the shear modulus (μ) ranges from 0.89 GPa to 1.42 GPa "Fig.11b". Shear modulus values from both layers reflect fairly to good competent material.

- **Young's modulus (E)**

Young's modulus (E) is estimated in terms of shear modulus (μ) and Poisson's ratio (σ) [6], [24], [25] as follows:

$$E = 2\mu(1+\sigma) \qquad (7).$$

In our study, Young's modulus (E) exhibits values from 1.29 GPa to 2.50 GPa in the first layer "Fig.10c" while, in the second layer, Young's modulus (E) ranges from 2.30 GPa to 2.85 GPa "Fig.11c". The values ranges of Young's modulus for both layers reveal fairly to good competent material.

- **Bulk modulus (K)**

We calculated the bulk's modulus in terms of Young's modulus and Poisson's ratio as follow [6]:

$$K = E/3(1-2\sigma) \qquad (8).$$

In this work, Bulk's modulus (B) exhibits values from 0.74 GPa to 1.55 GPa in the first layer "Fig.10d" reflecting fairly competent material while, in the second layer, Bulk's modulus (E) ranges from 1.84 GPa to 2.97 GPa "Fig.11d" reflecting good competent material.

C. Competence scales.

In order to evaluate the subsurface competence for proposed constructions, some of near-surface soil geotechnical parameters were calculated. These parameters are the Material Index (M_i), the Concentration Index (C_i), the Stress Ratio (S_i) and the Density Gradient (D_i).

- **Material index (M_i)**

The material index (M_i) shows to which degree the material is based on the elastic moduli and used as an investigation tool to evaluate soils for foundation purposes. The material index is related to the composition of the material, the solidification degree, the jointing, and rupture and the absence or presence of liquid in the pore spaces which affects the wave velocity. The material index is given in terms of Poisson's Ratio (σ) [6], [26], [27] as follows:

$$M_i = (1-4\sigma) \qquad (9).$$

In this study, the material index (M_i) exhibits values from (-0.240) to (0.174) in the first layer "Fig.12a" while, in the second layer, the material index (M_i) ranges from (-.450) to (-.097) "Fig.13d" which reflects fairly to moderately competent rock.

- **Concentration index (C_i)**

The degree of soil compaction is greatly considered as a measure of the competence degree for foundation works and other civil engineering activities. The concentration index (C_i) describes the material concentration degree. It depends mainly on the elastic moduli and the pressure distribution [26]. The concentration index can be given in terms of velocity squared ratio as stated by [28]:

$$C_i = (3 - 4\alpha)/(1 - 2\alpha) \qquad (10).$$

Where: α is the velocity squared ratio = (V_s^2/V_p^2). The ranges of Concentration Index (C_i) are summarized by [26]corresponding to soil competent degree "Table.2" In the study area, the concentration index (C_i) exhibits values from 4.23 to 5.84 in the first layer "Fig.12b" while, in the second layer, the concentration index (C_i) ranges from 3.76 to 4.65 "Fig.13b". The values of the concentration index (C_i) for both layers reflect fairly competent to competent soil.

- **Stress ratio (S_i)**

The consolidation settlement occurs during the excess pressure by a stress change. By the end of this solidification process, the overabundance load is almost zero and the stress change will have gone from a total state to an effective one. In this state, soil conditions are known as conditions for a stable equilibrium state which has zero horizontal and vertical strains[28]There is a relationship between Poisson's ratio (σ) and stress ratio (S_i) for normally consolidated soils. This relationship was given by[28] and [29] as follows:

$$Si = \sigma / (1-\sigma) \qquad (11).$$

The distribution of (Si) of the first layer in the study area as shown in "Fig.12c" reflects fairly to good competent soil, which is ranging from 0.26 to 0.45. On the other hand, the second layer reflects fairly competent soil which has Stress ratio values ranging from 0.37 to 0.56 "Fig.13c".

- **Density gradient (D_i)**

The density gradient (Di) is related to the consolidation settlement degree. [30] expressed the density gradient (D_i) in terms of P-wave and S-wave velocities as:

$$D_i = (V_p^2 - \frac{4}{3}V_s^2)^{-1} \qquad (12).$$

The calculated density gradient (D_i) exhibits low values for both the first layer "Fig.12d" and the second layer "Fig.13d" The low values reflect high competent materials [6]. The second layer is more competent according to the density gradient point of view.

D. Foundation bearing capacities.

The bearing capacity of earth materials is a very important and controlling engineering parameter when assessing or evaluating the subsurface conditions.

- **Ultimate bearing capacity (Q_{ult})**

The ultimate bearing capacity (Q_{ult}) of rock is defined as the maximum

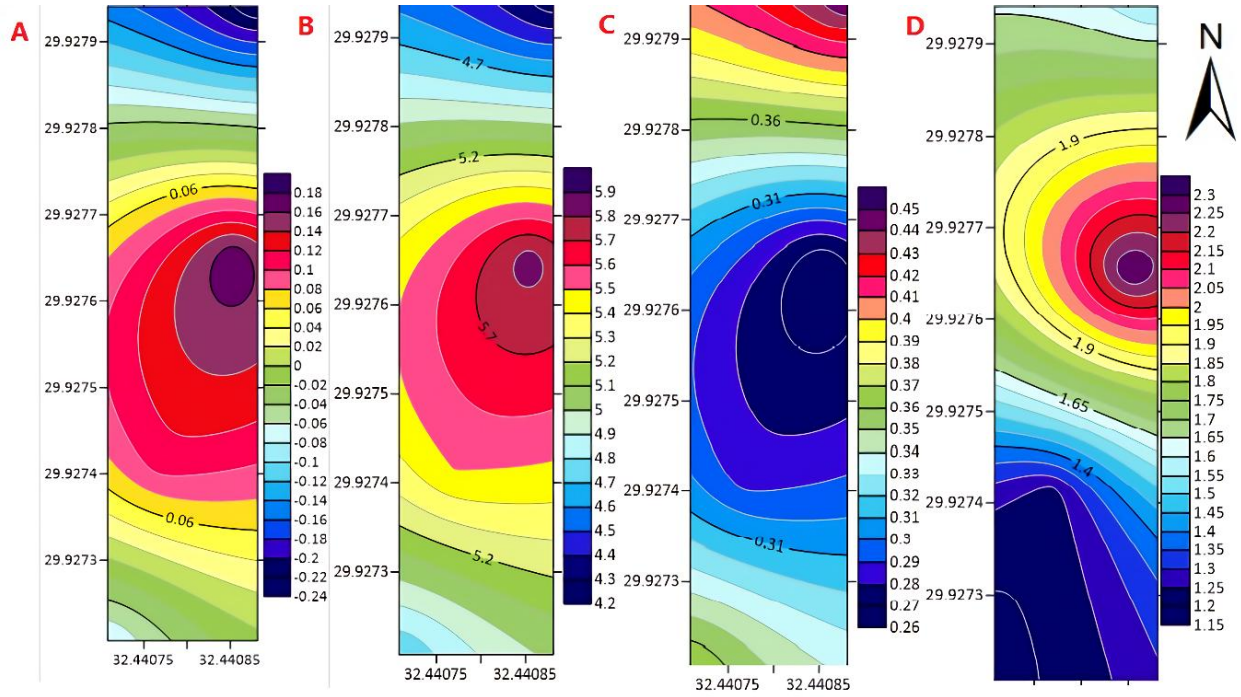

Fig.12 The lateral distribution of Competence scales for the first layer (a): Material index, (b): Concentration Index, (C): Stress Ratio, and (d): Density Gradient.

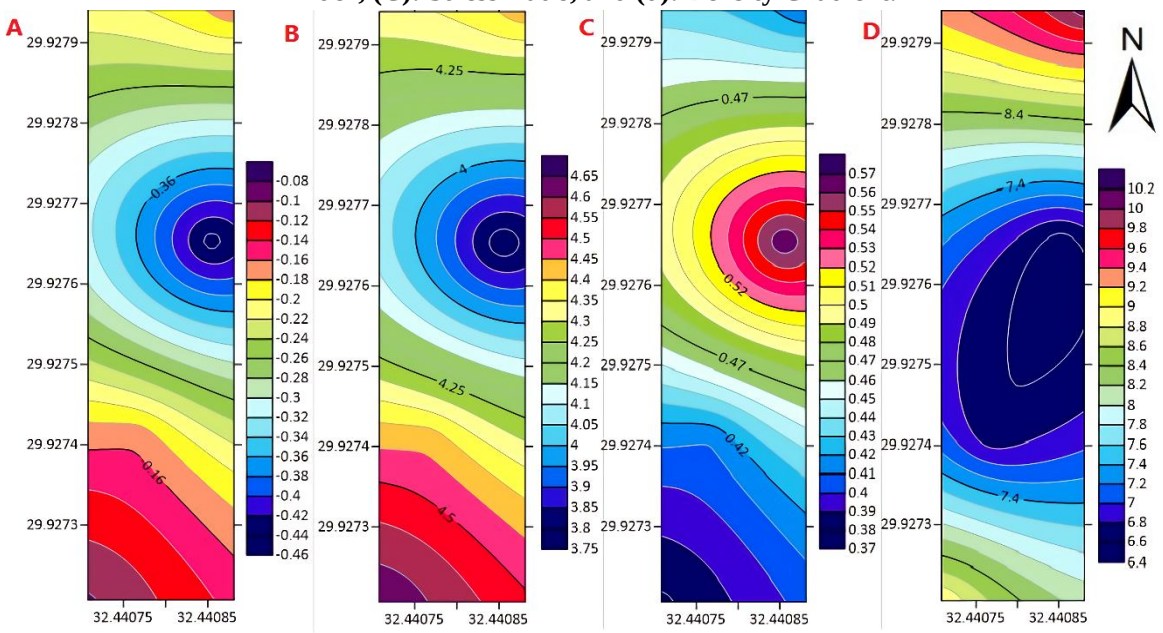

Fig.13 The lateral distribution of Competence scales for the second layer (a): Material index, (b): Concentration Index, (C): Stress Ratio, and (d): Density Gradient.

load required to cause fractures in it or break it. The ultimate bearing capacity (Q_{ult}) is related to the S-wave velocity and the bulk density through the following equation [27]:

$$Q_{ult} = (\rho * V_S)/100 \qquad (13)$$

Where ρ is the density in gm/cc, Vs is the shear wave velocity in m/s and Q_{ult} is the ultimate bearing capacity in Kg/cm^2. The ultimate bearing capacity (Q_{ult}) in the first layer ranges from 9.3 kg/cm^2 to 13.8 kg/cm^2 "Fig.14a"while, in the second layer ranges from 12.8 kg/cm^2 to 16.8.8 kg/cm^2 "Fig.15a".These results reflect the good bearing capacities of the subsurface.

- **Allowable bearing capacity (Q_{all})**

The allowable bearing capacity (Q_{all}) is calculated by dividing the ultimate bearing capacity by a safety factor (F) as follows:

$$Q_{all} = Q_{ult} / F \qquad (14).$$

We used a factor of safety equals (3) in this study. The allowable bearing capacity (Q_{all}) in the first layer ranges from 3.1 kg/cm^2 to 4.6 kg/cm^2 "Fig.14b" while, in the second layer ranges from 4.2 kg/cm^2 to 5.6 kg/cm^2 "Fig.15b" These values indicate that both layers are suitable for erecting the proposed structures.

Table- I Soil description with respect to Poisson's ratio and material index [28].

Description / Parameters	Incompetent to slightly competent	Fairly to moderately competent	Competent materials	Very high competent
Poisson's Ratio	0.41–0.49	0.35–0.27	0.25–0.16	0.12–0.03
Material Index	(-0.5) to (-1)	(-0.5) o (0.0)	0.0–0.5	>0.5

Table- II: Ranges of Concentration Index and Stress Ratio corresponding to the soil competent degree[27].

Soil description parameters	Weak		Fair		Good
	Incompetent		Fairly competent		Competent
	Very Soft	soft	Fairly compacted	Moderate compacted	Compacted
Concentration Index	3.5-4.0	4.0-4.5	4.5-5.0	5.0-5.5	5.5-6.0
Stress Ratio	0.7-0.61	0.61–0.52	0.52–0.43	0.43–0.34	0.34–0.25

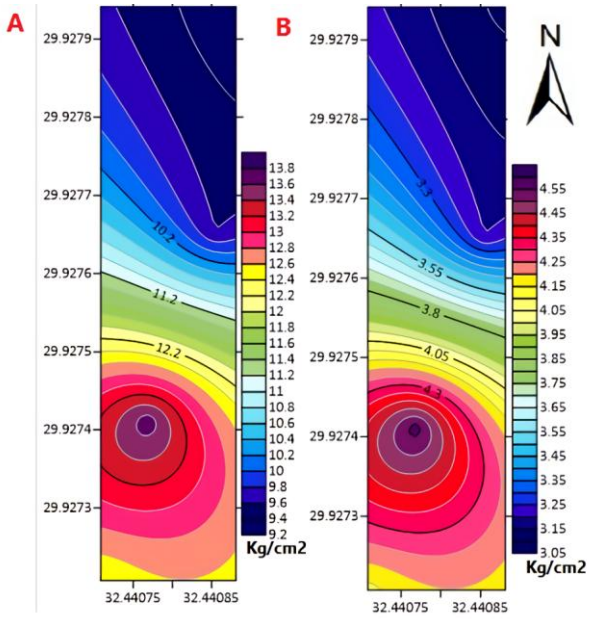

Fig.14 (A) Distribution map of foundation ultimate bearing capacity (Q_{ult}) (B) Allowable bearing capacity (Q_{all}) for the first layer.

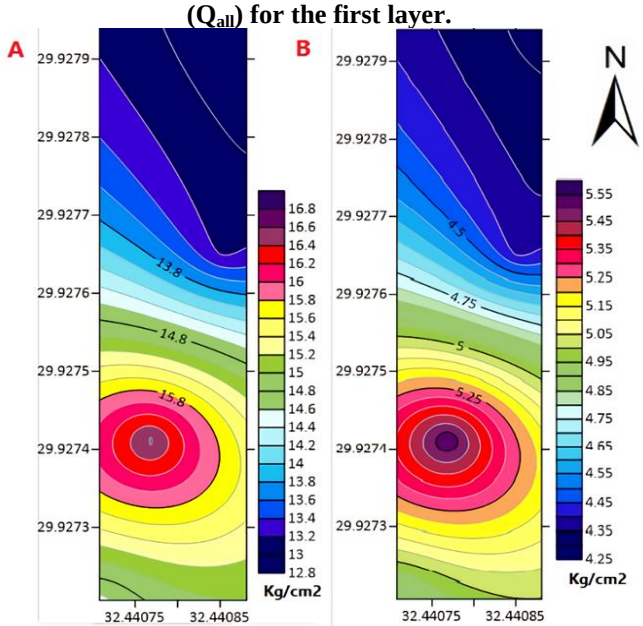

Fig. 15 (A) Distribution map of foundation ultimate bearing capacity (Qult) (B) Allowable bearing capacity (Qa) for the second layer.

VII CONCLUSIONS

The interpretation of the processed data which were obtained from the four seismic refraction and Multichannel analysis of surface waves (MASW) profiles converts the time-distance curves to velocity-depth models and subdivides the concerned depth seismically into two layers. The first layer is a thin surface layer ranges in thickness from 1 to 4 meters with P-wave velocity ranges from 924 m/s to 1247 m/s and S-wave velocity ranges from 530 m/s to 745 m/s. The compressional and shear wave velocities increase towards the central parts and decrease in the northeast direction. The second layer has a P-wave velocity ranges from 1277 m/s to 1573 m/s and S-wave velocity ranges from 684 m/s to 853 m/s. It was shown that the compressional and shear wave velocities increase towards the central parts and decrease in the northeast direction. The geotechnical parameters obtained from seismic velocities indicate that the first layer has acceptable competence properties and bearing capacities range from 9.3 kg/cm^2 to 13.8 kg/cm^2 .which is suitable for proposed structures which need bearing capacities about 2 kg/cm^2, so there is no need for removing the first layer.

Finally, we recommend that the competence zones distribution identified from the seismic data should be taken into consideration during the design of the structure stage and the foundation loads for the distribution of constructions and utilities.

REFERENCES

1. O. B. Olatinsu, K. F. Oyedele, and A. A. Ige-Adeyeye, "Electrical resistivity mapping as a tool for post-reclamation assessment of subsurface condition at a sand-filled site in Lagos, southwest Nigeria," SN Appl. Sci., vol. 1, no. 1, p. 24, Jan. 2019.
2. X. Wang, "Uncertainty quantification and reduction in the characterization of subsurface stratigraphy using limited geotechnical investigation data," Undergr. Sp., no. xxxx, Jan. 2019.
3. S. Rezaei, I. Shooshpasha, and H. Rezaei, "Empirical Correlation between Geotechnical and Geophysical Parameters in a Landslide Zone (Case Study: Nargeschal Landslide)," Earth Sci. Res. J., vol. 22, no. 3, pp. 195–204, Jul. 2018.
4. A. O. Oladotun, J. E. Oluwagbemi, A. M. Lola, O. Maxwell, and A. Sayo, "Predicting dynamic geotechnical parameters in near-surface coastal environment," Cogent Eng., vol. 6, no. 1, pp. 1–10, Mar. 2019.

5. E. Pegah and H. Liu, "Application of near-surface seismic refraction tomography and multichannel analysis of surface waves for geotechnical site characterizations: A case study," Eng. Geol., vol. 208, pp. 100–113, 2016.
6. S. Shebl, K. S. Gemail, M. Attwa, S. A. Soliman, A. Azab, and M. H. Farag, "Utilizing shallow seismic refraction in defining the geotechnical properties of the foundation materials: A case study at New Minia City, Nile Valley, Egypt," Egypt. J. Pet., Jan. 2019.
7. R. G. Sastry and S. Chahar, "Geoelectric versus MASW for geotechnical studies," J. Earth Syst. Sci., vol. 128, no. 2, pp. 1–13, 2019.
8. M. E. Mohamed Adel, A. Deif, S. El-Hadidy, S. R. Moustafa Sayed, and A. El Werr, "Definition of soil characteristics and ground response at the northwestern part of the Gulf of Suez, Egypt," J. Geophys. Eng., vol. 5, no. 4, pp. 420–437, 2008.
9. M. M. El Osta, A. El El Sheikh, and M. S. Barseem, "Comparative hydrological and geoelectrical study on the quaternary aquifer in the deltas of Wadi Badaa and Ghweiba, El Ain El Sukhna area, northwest suez gulf, Egypt," Int. J. Geophys., vol. 2010, no. 1, 2010.
10. K. M. A. Elenean, A. M. E. Mohamed, and H. M. Hussein, "Source parameters and ground motion of the Suez-Cairo shear zone earthquakes, Eastern Desert, Egypt," Nat. Hazards, vol. 52, no. 2, pp. 431–451, 2010.
11. A. G. A. Hewaidy, E. A. El-Motaal, S. A. Sultan, T. M. Ramdan, A. A. El khafif, and S. A. Soliman, "Groundwater exploration using resistivity and magnetic data at the northwestern part of the Gulf of Suez, Egypt," Egypt. J. Pet., vol. 24, no. 3, pp. 255–263, 2015.
12. S. A. S. Araffa, A. M. E. Mohamed, and F. M. Santos, "Geophysical investigation in the Northwestern part of the Gulf of Suez, Egypt," Egypt. J. Pet., vol. 26, no. 2, pp. 457–475, Jun. 2017.
13. ALBARQAWY Consulting Engineers laboratories, "Geotechnical report for the possibility of the area for construction purposes at ELCO Steel Rolling Factory, Ataqa Industrial Area, Suez., unpublished report," 2018.
14. K. Wittig, T. Ryberg, and M. H. Weber, "New insights into the seismic time term method for heterogeneous upper mantle slowness structures," GEM - Int. J. Geomathematics, vol. 8, no. 1, pp. 43–56, Apr. 2017.
15. Geometrics and OYO, SeisImager Manual. 2009.
16. C. B. Park, R. D. Miller, J. Xia, and J. Ivanov, "Multichannel analysis of surface waves (MAtSW) - Active and passive mehods," Lead. Edge (Tulsa, OK), vol. 26, no. 1, pp. 60–64, 2007.
17. J. Taipodia, A. Dey, and D. Baglari, "Influence of data acquisition and signal preprocessing parameters on the resolution of dispersion image from active MASW survey," J. Geophys. Eng., vol. 15, no. 4, pp. 1310–1326, 2018.
18. C. B. Park, R. D. Miller, J. Xia, and K. G. Survey, "Imaging dispersion curves of surface waves on multi-channel record," SEG Technical Program Expanded Abstracts 1998. Society of Exploration Geophysicists , pp. 1377–1380, 1998.
19. K. Hayashi, "Data Acquisition and Analysis of Active and Passive Surface Wave Methods." pp. 1–106, 2003.
20. G. H. F. Gardner, L. W. Gardner, and A. R. Gregory, "formation velocity and density—the diagnostic basics for stratigraphic traps," GEOPHYSICS, vol. 39, no. 6, pp. 770–780, Dec. 1974.
21. B. Sjögren, Shallow Refraction Seismics. Dordrecht: Springer Netherlands, 1984.
22. R. H. Tatham, "Vp/Vs and lithology," GEOPHYSICS, vol. 47, no. 3, pp. 336–344, Mar. 1982.
23. M. N. Toksöz, C. H. Cheng, and A. Timur, "velocities of seismic waves in porous rocks," GEOPHYSICS, vol. 41, no. 4, pp. 621–645, Aug. 1976.
24. W. Lowrie, Fundamentals of Geophysics. Cambridge: Cambridge University Press, 2007.
25. S. A. S. Araffa, A. M. E. Mohamed, and F. M. Santos, "Geophysical investigation in the Northwestern part of the Gulf of Suez, Egypt," Egypt. J. Pet., vol. 26, no. 2, pp. 457–475, Jun. 2017.
26. M. H. Khalil and S. M. Hanafy, "Engineering applications of seismic refraction method: A field example at Wadi Wardan, Northeast Gulf of Suez, Sinai, Egypt," J. Appl. Geophys., vol. 65, no. 3–4, pp. 132–141, Sep. 2008.
27. A. M. Abudeif, A. E. Raef, A. A. Abdel Moneim, M. A. Mohammed, and A. F. Farrag, "Dynamic geotechnical properties evaluation of a candidate nuclear power plant site (NPP): P- and S-waves seismic refraction technique, North Western Coast, Egypt," Soil Dyn. Earthq. Eng., vol. 99, no. April 2015, pp. 124–136, Aug. 2017.
28. J. E. Bowles, "Foundation Analysis and Design," Eng. Geol., vol. 20, no. 3, p. 587, Aug. 1982.
29. L. Thomsen, "Weak elastic anisotropy," GEOPHYSICS, vol. 51, no. 10, pp. 1954–1966, Oct. 1986.
30. H. stumpel, S. kahler, R. meissner, and B. milkereit, "the use of seismic shear waves and compressional waves for lithological problems of shallow sediments," Geophys. Prospect., vol. 32, no. 4, pp. 662–675, Aug. 1984.

AUTHORS PROFILE

Professor Maher A. Mesbah, has graduated his B.Sc. from geology department, Zagazeg University in 1983. In 1985 he obtained higher diploma studies from physics department, Alexandria University. His M.Sc. and Ph.D. were finished in 1988 and 1993, respectively from Alexandria University. Dr. Mesbah started his working carrier in 1985 at Alexandria University as a research student. Then, he joined NRIAG in 1989 as a researcher assistant and worked at Faculty of Petroleum and Mining Engineering at Suez as lecturer (1994), associate professor (1999) and professor of applied geophysics since 2004 tell now. He served as Vice-Dean, Dean and Vice President at Suez Canal University. Dr. Mesbah was elected to be the first President of Suez University in 2012. He is the founder of the university, since he started with 6 faculties and leaved his position in 2017 adding 6 more faculties. Research centers, a center of excellency and technological incubators has been established.

Dr. Asem Salama has built up his career for 3 years experience in the Egyptian geological survey and 13 years at seismology department at the national research institute of astronomy and geophysics, Egypt. His works covers various geophysics tools include seismic refraction (MASAW, borehole), Veses (Schlumberger method), seismology and study of paleotsunami deposits in the north Egypt. He had his PhD from University of Strasbourg, Ecole et Observatoire des science de la Terra (EOST), France at 2017. His last geotechnical consult was for built up the longest Ionic tower in the North Africa in the new Egyptian administrative capital city.

Dr. Mohamed Abdellatif A. ALBARQAWY, Lecturer of Geotechnical Engineering, Geological and Geophysical Engineering Department, Faculty of Petroleum and Mining Engineering, Suez University. Has some researches in the fields of Geotechnical, Geological Building Materials and Groundwater. Dr. Mohamed is the co-founder, the owner and General Manager of one of the most famous consulting offices in Egypt: ALBARQAWY Consulting Engineers office which is Multidisciplinary in Engineering Consultations for different Civil Projects including commercial and Residential Building, Industrial Projects and Infrastructures. Dr. Mohamed is interested in geophysical exploration techniques and measurements especially which are forwarded to Engineering applications such as preconstructions investigations and rock quality assessment.

Eng. Eslam Mohamed Ali, a technical instructor at geophysical and geological Engineering seeking for a challenging opportunity to improve my teaching skills, acquire more and more experience in both practical and academic fields and transfer this knowledge to younger generations. He has graduated his Bachelor of Science in Engineering from Geological and Geophysical Engineering Department, Faculty of Petroleum and Mining Engineering, Suez University in 2016. Eng. Eslam starts his career as a teaching assistant at Faculty of Petroleum and Mining Engineering, Suez University in March 2018 and till now. He had participated in organizing "The 13th International Conference on Mining, Petroleum, and Metallurgical Engineering (MPM 13) in October 2019.